Journal of Catalysis 278 (2011) 310–320

Contents lists available at ScienceDirect

Journal of Catalysis

journal homepage: www.elsevier.com/locate/jcat

Effect of the activation atmosphere on the activity of Fe catalysts supported on SBA-15 in the Fischer–Tropsch Synthesis

Leonardo A. Cano, María V. Cagnoli, José F. Bengoa, Ana M. Alvarez, Sergio G. Marchetti *

CINDECA, CONICET, CICPBA, UNLP, Fac. Ciencias Exactas, Fac. Ingeniería. Calle 47, No. 257, 1900-La Plata, Argentina

ARTICLE INFO

Article history:
Received 9 September 2010
Revised 29 November 2010
Accepted 27 December 2010

Keywords:
Fischer–Tropsch Synthesis
Fe/SBA-15
Activation atmosphere
Mössbauer spectroscopy

ABSTRACT

An iron catalyst supported on SBA-15 was prepared and activated in H_2 stream and in synthesis gas (H_2:CO = 2:1) stream, in order to be used in the Fischer–Tropsch Synthesis. The different activation treatments led to different Fe species in fresh catalysts: α-Fe, Fe_3O_4 and Fe^{2+} diffused into the SBA-15 walls in H2-Fe/SBA-15 and χ-Fe_5C_2, Fe_3O_4 and Fe^{2+} in H2:CO–Fe/SBA-15. These initial differences in the "bulk" structure of the solids disappear when both catalysts are "working". However, a higher production of total hydrocarbons, higher CO conversion and more CH_4 and light gases were obtained for H2-Fe/SBA-15 over 6 days. Besides, a higher selectivity toward light olefins was obtained with H2-Fe/SBA-15 during the first 24 h on reaction stream, but this selectivity decreases with the reaction time. These results are explained considering that the iron carbides produced from α-Fe are more active and/or have smaller sizes than that obtained from α-Fe_2O_3.

1. Introduction

The Fischer–Tropsch Synthesis (FTS) is a process used to produce hydrocarbons from syngas (a mixture of H_2 and CO) [1,2]:

$$(2n+1)H_2 + nCO \rightarrow C_nH_{2n+2} + nH_2O$$

Different metals are active as catalysts in the FTS, but today, Co and Fe are the only reasonable commercial catalysts for this process [3]. When iron is used as catalyst, the FTS occurs simultaneously with the water–gas shift (WGS) reaction. It consumes CO and water obtained from the FTS and produces additional H_2 and CO_2. For this reason, the iron catalysts are the best choice when a syngas poor in hydrogen is used. This situation occurs if the syngas is produced by gasification of coal or biomass. Besides, the iron catalysts are preferred to Co catalysts, since they have lower cost, lower methane selectivity, lower sensitivity to poisons, and higher flexibility to lead the selectivity to alkenes, oxygenates, or branched hydrocarbons according to the promoters or the operative variables used. For these reasons, the precipitated or fused iron catalysts (unsupported catalysts) have been extensively studied. However, the purpose of the activation pretreatment of these catalysts is not clearly understood yet. Reduction in pure H_2 may lead to α-Fe, but upon exposure to syngas, it is rapidly transformed to iron carbide phase or a mixture of iron carbide phases [4–6]. At high syngas conversions, the reaction mixture becomes more oxidizing and magnetite is also produced [4]. Therefore, during the FTS, the iron phase may be distributed between several species such as carbides, oxides, and metallic iron. As a consequence, it is very hard to determine a correlation between the catalyst composition and its activity and selectivity. Some authors have proposed that surface carbides are the active phase, with an underlying structure of bulk iron carbide [5,6]. In the so-called competition model, proposed by Niemantsverdriet and van der Kraan [7], iron atoms at the surface are considered as the active sites, and the bulk diffusion of carbon into metallic iron and hydrocarbon synthesis have a common surface carbidic C^*. Other researchers have proposed that Fe_3O_4 is the active phase in FTS [8,9]. There is evidence questioning [10,11] and supporting [12–14] this proposal.

Taking into account the previous description, it can be concluded that the activation pretreatments have an important influence on the FTS activity and selectivity when iron is used as catalyst. For this reason, there are many articles dealing with the effect of the activation conditions on the performance of iron catalysts, in particular when unsupported iron is used. In this way, Pennline et al. [15] found that coprecipitated Fe–Mn catalysts were nearly inactive when they were pretreated with pure H_2 or syngas and they only showed activity if they were activated with pure CO. Instead, Bukur et al. [16,17] have noticed that unsupported Fe/Cu/K catalysts were more active when they were pretreated with pure

Abbreviation: FTS, Fischer–Tropsch Synthesis.

* Corresponding author. Fax: +54 221 4210711.
E-mail addresses: lcano@quimica.unlp.edu.ar (L.A. Cano), mavic@quimica.unlp.edu.ar (M.V. Cagnoli), bengoajf@quimica.unlp.edu.ar (J.F. Bengoa), anamalvz@quimica.unlp.edu.ar (A.M. Alvarez), march@quimica.unlp.edu.ar (S.G. Marchetti).

0021-9517/$ - see front matter © 2010 Elsevier Inc. All rights reserved.
doi:10.1016/j.jcat.2010.12.017

H_2, but they produced a higher quantity of CH_4 and light hydrocarbons. On the other hand, O'Brien et al. [18,19] have worked with unsupported Fe/Si/K catalysts and they found that the activation process at high pressure had a detrimental effect on the catalytic behavior and the highest conversions were obtained when the activation was done in pure CO. Similar results were obtained by Luo et al. [3] with precipitated Fe/Si/K catalysts.

As can be seen from this brief review, the activation studies have been done mainly with unsupported iron catalysts, and the results are contradictory since they have a strong dependence on the structural characteristics of the solid precursors, the number and the nature of the promoters, etc.

To our knowledge, the bibliography focused on the influence of the activation pretreatments is scarce when supported iron catalysts are used. One article reporting the use of iron moderately dispersed on SiO_2 was published by Xu and Bartholomew [20]. These authors found that the initial activity changes with the activation atmosphere following the sequence $H_2 > H_2$:CO = 1 > CO. Besides, the amount of reactive atomic surface carbon (C_α) increases with increasing H_2 content in pretreatment gas. The development of supported iron catalysts is highly desirable since the most economical reactors in FTS are the slurry bubble columns, in which the unsupported iron catalysts undergo attrition at high velocity, leading to a catalyst loss and an increase in slurry viscosity.

On the other hand, it would be possible to increase the selectivity of the synthesis by controlling the crystal size of the active phase. This method is based on the fact that in some heterogeneous catalytic reactions, the activity of the solid is a function of the crystal size of the active phase, generally in the 1–10 nm range. These reactions are known as "structure sensitive" [21]. In the literature, there is some early evidence that the FTS is "structure sensitive" [22], and more recently, this property would be confirmed by using supported Co and Fe catalysts [23–25]. Today, the concept of "structure sensitive" involves the activity and selectivity of the catalyst. This idea was recently verified by Bezemer et al. [26] using Co particles with sizes between 2.6 and 27 nm supported on carbon nanofibers. These authors found that when the cobalt particle size was reduced from 16 to 2.6 nm, the turnover frequency for CO hydrogenation decreased about twenty times, while C_{5+} selectivity decreased from 85 to 51 wt.%. Therefore, it would be possible to achieve an improvement in the catalyst selectivity if particles of supported Fe oxides, with a determined average diameter and a narrow size distribution, were obtained. In order to get this scope, an "inert" support with a narrow pore-size distribution and thermal stability would be selected. Besides, the pore diameters of the support must be large enough to locate the iron oxide crystals inside the pores, avoiding their migration to the outer surface during the activation steps. The mesoporous solid named SBA-15 seems to fulfill the above conditions since it has a narrow pore-size distribution, with a hexagonal arrangement, whose diameters can be varied between 5 and 30 nm, wall thickness between 3 and 6 nm, and specific surface area between 700 and 1000 m^2/g [27,28]. The use of this type of support is not enough to obtain a narrow crystal-size distribution in the desired size range of the active Fe species. In order to get this scope, it is necessary to introduce the total iron loading inside the support channels avoiding its migration to the outer surface when the catalyst is "working" since the controlling effect on the sintering process would be lost. Achieving these objectives represents a real challenge.

Taking into account all previous considerations, the aim of the present work is to obtain an Fe/SBA-15 catalyst controlling the crystal sizes of the iron species and to analyze the effect of the activation atmosphere on the activity and selectivity of this catalyst in the FTS.

2. Experimental

2.1. Catalyst preparation

The SBA-15 support was synthesized according to the methodology proposed by Zhao et al. [27,28] using Pluronic triblock copolymer P123 (EO20-PO70-EO20) as organic structure-directing agent and tetraethyl orthosilicate (TEOS) as silica source. Thus, 12 g of Pluronic P123 was dissolved in 360 ml of water and 60 ml of HCl solution (37%, w/w) with stirring at 313 K for 3 h. Then, 27 ml of TEOS was added, and the solution was kept stirring at 313 K for 24 h. The mixture was aged at 363 K overnight, without stirring. The solid was recovered by filtration, washed, and dried in air at room temperature (RT). Calcination in air was carried out from RT to 773 K at 1 K/min and kept at 773 K for 6 h.

SBA-15 was impregnated by the incipient wetness impregnation method with $Fe(NO_3)_3{\cdot}9H_2O$ ethanolic solution to produce a nominal Fe loading of 15% w/w in a single step. The solid Fe/SBA-15 was dried using a rotary evaporator at 313 K for 24 h and finally calcined in a flow of NO (1% v/v)/He (100 cm^3/min) from RT to 723 K at a heating rate of 1 K/min and kept at this temperature for 4 h. The sample thus obtained was called p-Fe/SBA-15. A fraction of this precursor was activated in H_2 flow (60 cm^3/min) by heating from RT to 703 K for 80 min and kept at this temperature for 26 h. This solid was called H2-Fe/SBA-15. The other fraction of the precursor was activated in H_2/CO (2:1) flow (20 cm^3/min) by heating from RT to 703 K for 80 min. This solid was called H2:CO–Fe/SBA-15. When the activation processes were completed, the catalytic test began.

2.2. Catalyst characterization

The samples were characterized by atomic absorption spectroscopy (AAS), X-ray diffraction (XRD) at low angles, N_2 adsorption (BET), Mössbauer spectroscopy (MS) at 298 and 30 K, and temperature-programmed hydrogenation (TPH).

The Fe content of the solid was determined by atomic absorption on an AA/AE Spectrophotometer 457 of Laboratory Instrumentation Inc. The sample was attacked in a mixture of HCl and HF up to complete dissolution and then was treated according to conventional methods for this technique.

The X-ray diffraction patterns at low angles were recorded in Shimadzu equipment, XD3A model, using Cu Kα radiation generated at 40 kV and 40 mA in the range $2\theta = 0.5–9^\circ$ with steps of 0.02° and counting time of 2 s/step.

The textural properties, specific surface area (S_g), specific pore volume (V_p) and pore diameter (D_p), were measured in Micromeritics equipment ASAP 2020 V1.02 E.

The Mössbauer spectra were obtained in transmission geometry with a 512-channel constant acceleration spectrometer. A source of ^{57}Co in Rh matrix of nominally 50 mCi was used. Velocity calibration was performed against a 12-μm-thick α-Fe foil. All isomer shifts (δ) mentioned in this paper are referred to this standard. The temperature was varied between 30 and 298 K using a Displex DE-202 Closed Cycle Cryogenic System. The Mössbauer spectra were evaluated using a commercial program with constraints named Recoil [29]. Although some spectra display magnetic relaxation, for simplicity, Lorentzian lines with equal widths were considered for each spectrum component. The spectra were folded to minimize geometric effects. The spectra of the activated and used samples were obtained in their corresponding activation atmospheres, using a cell specially built for this purpose, to be used inside the cryogenic system [30].

2.3. Activity and selectivity measurements

Activity and selectivity measurements in FTS were carried out in a stainless steel fixed-bed reactor (2.54 cm o.d.) at 703 K, at atmospheric pressure, with a H_2:CO ratio of 2:1 (premixture stored in a cylinder), a space velocity of 1176 h^{-1} (≈450 mg of catalyst and 20 cm^3/min of total flow). Before reaction, the precursors were activated *in situ* following the methodologies described above. A set of valves was used to select the required gases. These gases were passed through the following filtering elements (at RT): a Pd-based catalyst to remove residual O_2 and a molecular sieve to remove water traces. In addition, the mixture H_2:CO was passed through a filter (heated at 353 K) to remove some Fe or Ni carbonyl compounds formed in the gas bottle. All gas flows were measured and controlled by mass flow meters. The reaction products were analyzed online by gas chromatography using FID and TCD detectors with GS-Gas Pro capillary column and a HAYESEP DB 100/120 packed one, respectively. After the reactor, the tubing lines were kept at about 503 K to avoid product condensation. Alternatively, this hot stream went through a heated six-way injection valve that collected 1.8 ml of gas sample to be injected into the capillary column for hydrocarbons using a split ratio of 20:1 or through a second heated six-way valve, and the permanent gases were injected into the packed column. Under these catalytic conditions, heavy hydrocarbons and waxes were not produced; therefore, cold traps to collect these fractions were not necessary. It was established that the empty stainless steel reactor was inactive for the reaction under the test conditions.

In situ TPH tests were performed on the used catalysts, using a TCD detector. After keeping the catalysts under reaction conditions for 6 days, as will be described below, they were used for the TPH tests with a pure H_2 flow. The samples were cooled to RT in the reaction mixture, purged with pure H_2 (50 cm^3/min) at RT, and then the temperature was increased from RT to 1273 K at 20 K/min under pure H_2 flow. With this technique, all the carbonaceous species are converted to CH_4, allowing the distinction between various iron carbides and/or C surface species.

3. Results and discussion

The ordered hexagonal structure of mesoporous SBA-15, used as support, was verified by XRD (Fig. 1) and by its textural properties, measured by N_2 adsorption (Table 1). By combining the results of both techniques as in Ref. [31], the wall thickness was obtained.

The impregnation and calcination treatments, which lead to obtaining p-Fe/SBA-15, do not change the structural properties of the mesoporous support, as was verified by XRD (Fig. 1).

The iron nitrate was decomposed by calcination in a flow of NO (1% v/v)/He since it has recently been demonstrated by Sietsma et al. and den Breejen et al. [32,33] that calcination with NO flow produces Co particles with significantly smaller sizes in the Co/SiO_2 system when cobalt nitrate salt is used in the impregnation step. Besides, a significant narrowing in particle size distribution was obtained when NO flow was used instead of air flow. These results would be explained since NO is one of the nitrogen oxides produced during cobalt nitrate decomposition; therefore, if it is fed during the calcination process, the salt decomposition would occur in a controlled way and the clustering and growth of the nanoparticles would be avoided. Considering that the anion of our iron salt is the same, we expected a similar result with our system. The Mössbauer results that will be discussed below point in this direction.

By analyzing the textural properties, a decrease of V_p and S_g in comparison with the support, without substantial changes in D_p, can be observed. This would imply a partial pore filling of the support with the Fe oxide species (Table 1). The Fe content obtained by AAS is also shown in Table 1.

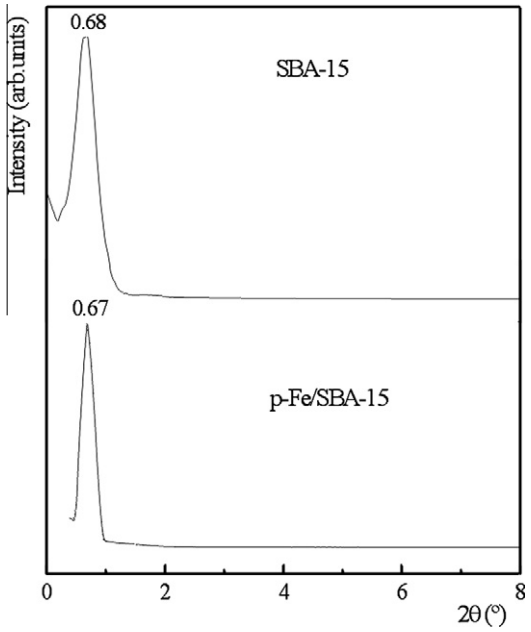

Fig. 1. XRD patterns at low angles of SBA-15 and p-Fe/SBA-15.

Table 1
Textural properties of SBA-15 and p-Fe/SBA-15.

	S_g[a] (m^2/g)	D_p[b] (nm)	V_p[c] (cm^3/g)	e[d] (nm)	Fe (% w/w)
SBA-15	893	8.1	1.09	7	–
p-Fe/SBA-15	519	7.1	0.57		13

[a] Specific surface area.
[b] Average pore diameter.
[c] Specific pore volume.
[d] Wall thickness.

The p-Fe/SBA-15 Mössbauer spectrum at 298 K (Fig. 2) displayed a doublet that could be assigned to superparamagnetic (sp) α-Fe_2O_3 and/or paramagnetic Fe^{3+} [34]. When the spectrum is measured at 30 K, six broad peaks are observed. They were fitted with a sextuplet with a hyperfine field distribution and a very small central doublet (4 ± 1%). The sextet has hyperfine parameters corresponding to α-Fe_2O_3 crystals that did not present the Morin transition (crystal size lower than about 20 nm) [35] and with its magnetic hyperfine field decreased due to the crystal-size effect (Table 2). In order to determine the value of blocking temperature T_B (defined as the temperature at which 50% of the sextet component has collapsed to a doublet), the Mössbauer spectra at intermediate temperatures between 298 and 30 K were obtained (Fig. 2 and Table 2). Taking into account that at 100, 80, and 60 K the superparamagnetic relaxation phenomenon is present (when the temperature decreases, the disappearance of the curved background and the "freezing" of the relaxing magnetization vector can be seen), the different interactions were fitted using the relaxation model of Blume and Tjon [36]. In this way, a T_B value of 100 K was determined. The spectra at 60, 45, and 30 K showed the same percentage (within the experimental errors) of the doublet signal: 4 ± 1%. Therefore, it can be concluded that this signal corresponds to a small fraction of paramagnetic Fe^{3+} diffused inside the walls of the SBA-15 support. By applying the Neel-Brown relaxation model [37] and using a basal anisotropy constant $K_{BU} = 2.4 \times 10^4$ J/m^3, determined by Bødker and Mørup [38] for

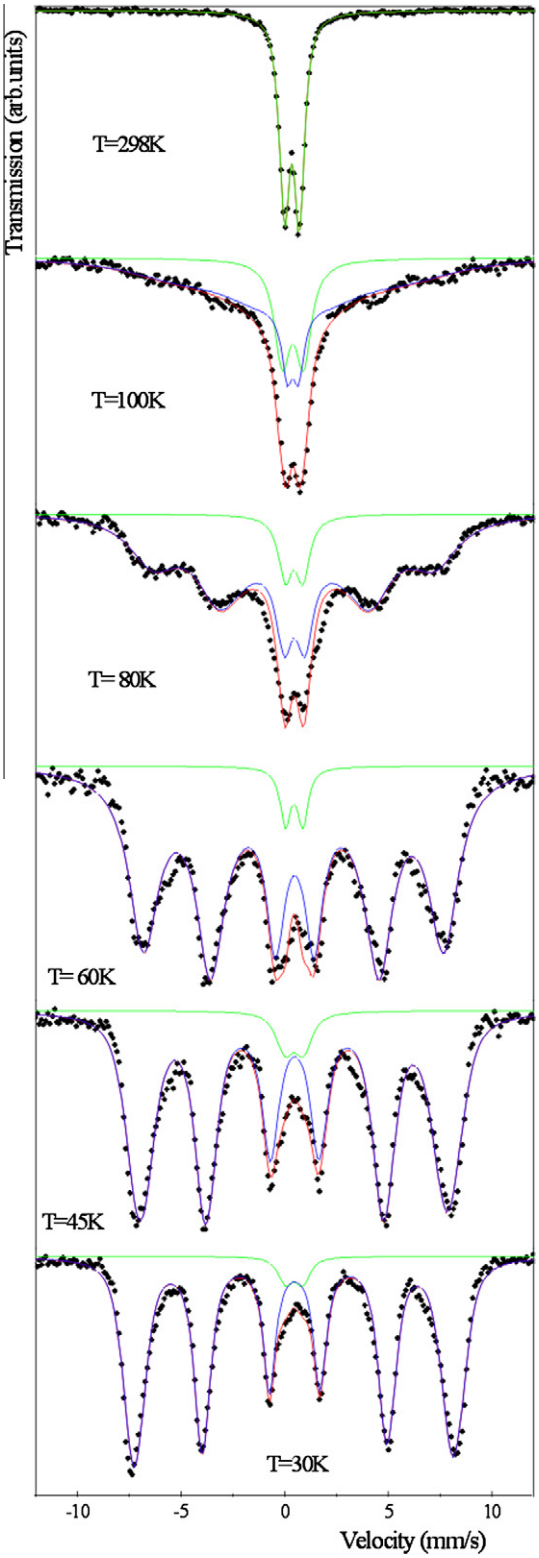

Fig. 2. Mössbauer spectra of p-Fe/SBA-15 at 298, 100, 80, 60, 45, and 30 K.

hematite particles of 5.9 nm size, an estimation of the average diameter value of crystal oxide of about 8 nm was obtained. There is a complete coincidence between this value and the diameter of the SBA-15 channels. Bearing in mind the numerous assumptions of the models used, this coincidence would seem to be fortuitous. However, if we consider this result jointly with the textural measurements and with the fact that at room temperature the Mössbauer spectrum did not show any magnetic signal, we can conclude that the total iron loading is located inside the SBA-15 channels. Besides, the iron oxide has a narrow size distribution with an average diameter of about 8 nm.

In order to establish the most adequate reaction temperature for FTS when the Fe/SBA-15 system is used as catalyst, the precursor p-Fe/SBA-15 was activated in pure H_2 and H_2:CO = 2:1 mixture, following the procedures previously described. Preliminary catalytic tests for both solids (H2-Fe/SBA-15 and H2:CO–Fe/SBA-15 respectively) were realized at four temperatures, 543, 603, 653, and 703 K, in a consecutive way without changing the catalyst loading and remaining in continuous reaction at least 24 h at each temperature. Fig. 3 shows the production of total hydrocarbons (HC molecules/g Fe. s), the CO conversion (%), and CH_4 selectivity, defined as:

$$\frac{[CH_4 \cdot \text{moles} \times C \cdot \text{number of } CH_4] \times 100}{\sum_{i+1}^{n}[\text{“}i\text{”} \text{ moles} \times C \text{ number of } C_i]}$$

The activity of these catalysts could be expressed as the turnover rate. In order to obtain this expression, it would be necessary to measure the available surface metallic iron on fresh catalysts. However, the metallic iron changes rapidly under the synthesis conditions. Therefore, this expression appears inappropriate for iron catalysts. To solve this difficulty, the group led by Iglesia proposed a new method, measuring irreversible CO chemisorption on used catalysts, to provide a quantitative measurement of active sites [39], but in a subsequent article published by Xu and Bartholomew [20], it was demonstrated that this method does not provide good results on silica-supported iron. Therefore, further research appears as necessary to solve this problem, and we chose the above expression to evaluate the activity of the present catalysts. The results showed that the production of total hydrocarbons per gram of iron increased 50–100 times and the CO conversion increased 70–350 times, for both catalysts, when the reaction temperature was increased from 543 to 703 K. However, it is important to remark that the major change occurs between 653 and 703 K. If the global reaction rate was controlled by the diffusion rate inside the channels of the SBA-15 support, the catalytic activity would be expected to change in a proportional way with approximately $T^{3/2}$. We think that at temperatures $\leqslant$653 K, the reaction occurs on the iron crystals located at the mouth of the pores, since these crystals inhibit the CO access and/or the product exit. The H_2 access occurs since, as will be demonstrated below, all α-Fe_2O_3 disappears after reduction pretreatment with this gas. When the temperature reached the value of 703 K, the expansion of the mouth of the pores – produced by the different vibrational behaviors of the support and the active phase – would allow the CO access and/or the product exit. Therefore, under these conditions, the total metallic loading would be accessible and the production of total hydrocarbons per gram of iron and the CO conversion would be significantly increased. A similar behavior was observed in previous work using Fe/MCM-41 as catalyst [24]. In this system, we could determine, using STEM-HAADF images of the oxidic and reduced samples [40,41], that iron species are located along the channels as “nanocylinders” with diameters nearly equal to the channels of the mesoporous support. As a consequence, the empty spaces between the walls of the support and the iron “nanocylinders” are extremely small. Besides, in Fig. 3, it can be seen that CH_4 selectivity decreases when the reaction temperature increases. This effect is particularly noticeable in H2:CO–Fe/SBA-15 and shows that higher temperatures are necessary to get the chain growth when the Fe/SBA-15 system – with all iron loading located inside the channels of the support – is used as catalyst. It is important to remark that this required high reaction temperature is inappropriate for an industrial application, and

Table 2
Mössbauer parameters of p-Fe/SBA-15 at different temperatures.

Species	Parameters[a]	298 K	100 K	80 K	60 K	45 K	30 K
α-Fe_2O_3 (sp) and/or paramagnetic Fe^{3+}	Δ (mm/s)	0.72 ± 0.01	0.88 ± 0.02	0.9[b]	–	–	–
	δ (mm/s)	0.36 ± 0.01	0.45 ± 0.01	0.46[b]	–	–	–
	%	100 ± 1	52 ± 1	12 ± 1	–	–	–
Partially magnetically blocked α-Fe_2O_3	H (T)	–	44[b]	44.0 ± 0.3	45.7 ± 0.2	–	–
	δ (mm/s)	–	0.45[b]	0.46[b]	0.46 ± 0.01	–	–
	2ε (mm/s)	–	−0.13[b]	−0.07 ± 0.04	−0.05 ± 0.03	–	–
	%	–	48 ± 3	88 ± 2	96 ± 2	–	–
α-Fe_2O_3	H (T)	–	–	–	–	46.0 ± 0.1	47.7 ± 0.1
	δ (mm/s)	–	–	–	–	0.47 ± 0.01	0.46 ± 0.01
	2ε (mm/s)	–	–	–	–	−0.05 ± 0.02	−0.05 ± 0.01
	%	–	–	–	–	95 ± 1	96 ± 1
Paramagnetic Fe^{3+}	Δ (mm/s)	–	–	–	0.84[b]	0.9 ± 0.1	0.8 ± 0.1
	δ (mm/s)	–	–	–	0.46[b]	0.46[b]	0.46[b]
	%	–	–	–	4 ± 1	5 ± 1	4 ± 1

H: hyperfine magnetic field in Tesla.
δ: isomer shift (all the isomer shifts are referred to α-Fe at 298 K).
2ε: quadrupole shift.
Δ: quadrupole splitting.
[a] Hyperfine parameters.
[b] Parameters held fixed in fitting.

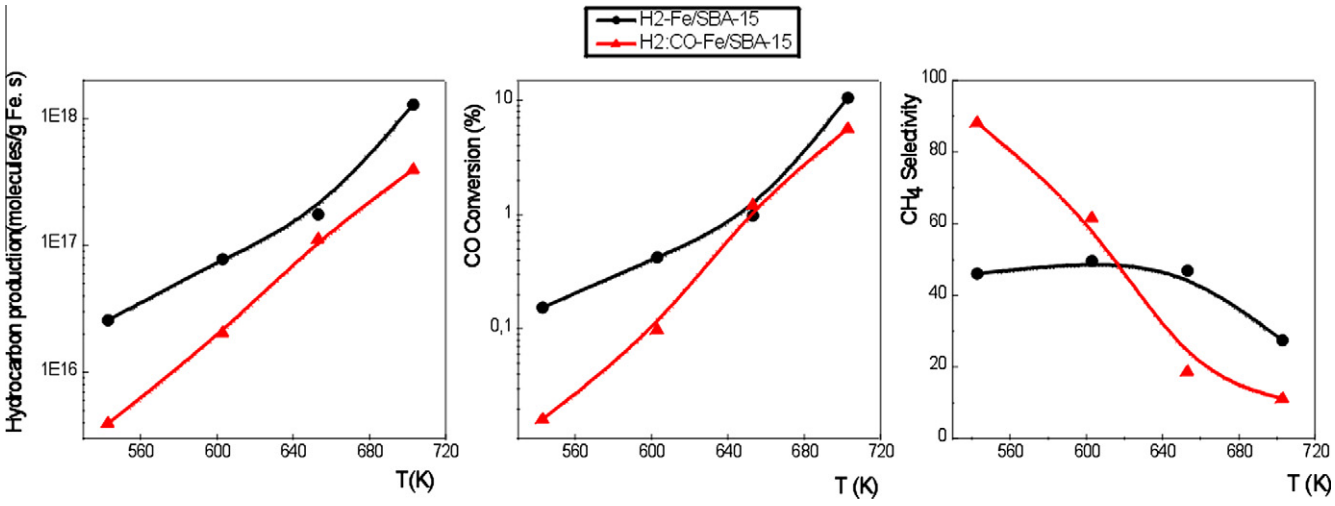

Fig. 3. Total hydrocarbon production (molecules/g Fe s), CO conversion (%), and CH_4 selectivity vs. reaction temperature for H2-Fe/SBA-15 and H2:CO–Fe/SBA-15. Solid lines are to guide the eye only.

some structural changes of the solids would be necessary, but the scope of the present work is not focused on this subject, and further work is in progress in this sense.

Once the most adequate FTS temperature was determined for these catalysts, two fresh samples were activated in pure H_2 and H_2:CO = 2:1 mixture, respectively, and the FTS was measured at 703 K in a continuous way for 6 days. Table 3 shows the catalytic results for both catalysts at three characteristic reaction times: at short reaction time (≈7 h), in the pseudo-stationary state (≈24 h), and at long reaction time (≈144 h). It can be seen that H2-Fe/SBA-15 has a total hydrocarbon production per gram of Fe about three times higher than H2:CO–Fe/SBA-15, all over the reaction time. A similar trend was observed for the total CO conversion percentage; compared to H2:CO–Fe/SBA-15, the activity of H2-Fe/SBA-15 increased about two times and for the CO conversion toward CO_2 about 1.5 times. In order to evaluate the selectivities of both catalysts, it is necessary to consider that the selectivity of the FTS is affected by CO conversion. Therefore, the selectivity comparison between both catalysts must be done at iso-conversion. On the other hand, it is well known that an increase in CO conversion produces a decrease in olefin selectivity [42]. Therefore, taking into account that in the present situation, the catalyst with higher conversion also produces more olefins (H2-Fe/SBA-15) up to the steady state, it can be inferred that the solid activated in pure H_2 is more selective toward the production of light olefins, regardless of the conversion differences at the first reaction days (Table 3). At long reaction time (144 h), it is not possible to obtain a conclusion about this topic under these conditions. Finally, a higher chain growth and a lower CH_4 production were found with H2:CO–Fe/SBA-15 (Fig. 4).

In order to explain the different catalytic behavior produced by the different activation process, we obtained the Mössbauer spectra of both catalysts at 298 and 30 K after the activation process – zero reaction time – and after reaching the pseudo-stationary state (24 h) under the FTS conditions. In both cases, after the corresponding process, the samples were "quenched", and the spectra were obtained in the same atmosphere of the treatment with a cell specially built by us for this purpose to be used inside the

Table 3
Activity and selectivity results obtained at 703 K and three different reaction times: at short reaction time (≈7 h), in the pseudo-stationary state (≈24 h), and at long reaction time (≈144 h).

	H2-Fe/SBA-15			H2:CO–Fe/SBA-15		
	[e] t_r = 465′	[e] t_r = 1592′	[e] t_r = 8517′	[e] t_r = 421′	[e] t_r = 1441′	[e] t_r = 8661′
Prod. HC_{totals} (molecules/g_{Fe}. s)[a]	13.2×10^{17}	17.3×10^{17}	23.5×10^{17}	4.3×10^{17}	5.7×10^{17}	7.0×10^{17}
R[b]	2.06	1.24	0.28	1.05	1.13	0.97
% CO_2[c]	–	8.3	–	–	5.4	–
X_{CO} (%)[d]	19.9	20.1	18.7	8.6	12.1	10.0

[a] Prod. HC_{totals}: hydrocarbons production per gram of Fe.
[b] R: $(C_2^= + C_3^=)/(C_2 + C_3)$.
[c] % CO converted to CO_2.
[d] X_{CO} (%): total CO conversion.
[e] t_r: reaction time.

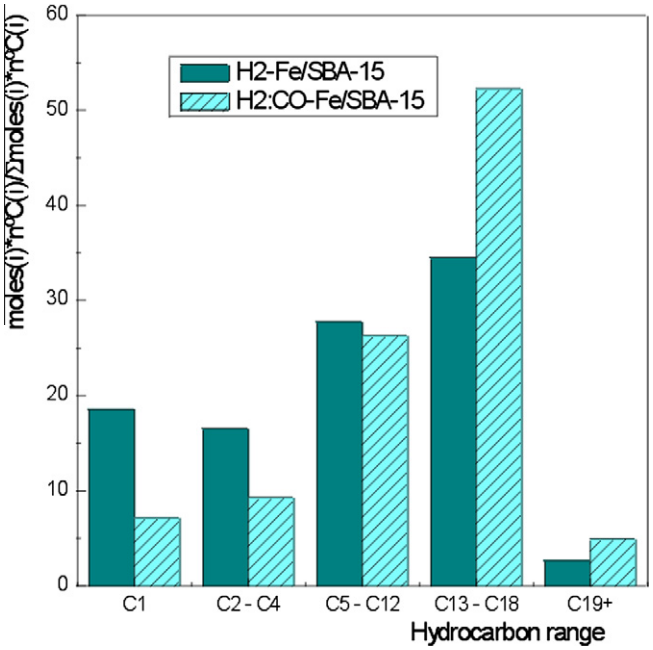

Fig. 4. Selectivity diagram for H2-Fe/SBA-15 and H2:CO–Fe/SBA-15, evaluated at 703 K in the pseudo-stationary state (≈24 h).

cryogenic system [30]. In this way, the samples never were contacted with air.

The Mössbauer spectra of the fresh catalysts at 298 K (Fig. 5) display an asymmetric doublet with a shoulder on the positive-velocity side and broad lines, which could be attributed to paramagnetic and/or superparamagnetic (sp) species. To carry out the species assignments, the Mössbauer spectra at 30 K were obtained. It is important to remark that due to the extreme complexity of the spectra at low temperature, a real fitting process was not carried out. Thus, initially, a set of hyperfine parameter distributions, typical of the possible species present, were fixed and the areas were fitted freely. When they converged to a minimum, the areas were fixed and the values of isomer shift (δ) and quadrupole splitting (Δ) of the doublets and the hyperfine magnetic fields (H) of the sextuplets were fitted freely. It was assumed that the hyperfine magnetic fields could decrease due to the effects of the crystal size, but the isomer shifts and the quadrupole shifts (2ε) were fixed, considering that these parameters would not be affected by this variable. It is possible that following this methodology, the fitting could produce more than one minimum, with very small differences between them. Therefore, to choose the best set of values, the story of the sample and physical and chemical concepts were used too. The H2:CO–Fe/SBA-15 spectrum at 30 K was fitted with five sextets for the five Fe_3O_4 crystallographic sites [43], three sextets assigned to the three sites of the χ-Fe_2C_5 carbide [44], and two doublets assigned to Fe^{2+} ions located in tetrahedral and octahedral sites within the walls of SiO_2 [45] (Table 4 and Fig. 5). They are present in a superparamagnetic regime or as paramagnetic species in the spectrum at 298 K: a doublet of carbide (sp) [44], a singlet of Fe_3O_4 (sp) [46], and two doublets assigned to paramagnetic Fe^{2+} ions diffused into the SiO_2 walls and/or Fe_3O_4 (sp) (Table 4). The steps of the fitting procedure for H2-Fe/SBA-15 Mössbauer spectrum at 30 K were the same as in H2:CO–Fe/SBA-15. The hyperfine parameters obtained following this methodology are shown in Table 4. The more important difference between both spectra is the presence of one sextet, which has hyperfine parameters typical of α-Fe, instead of the three sextets assignable to χ-Fe_2C_5 carbide. At room temperature, the α-Fe species is detected as a singlet due to the superparamagnetic behavior [45]. In Table 5, it can be seen that within the experimental errors, the percentages of α-Fe in H2-Fe/SBA-15 and χ-Fe_2C_5 carbide in H2:CO–Fe/SBA-15 are equal. Besides, the percentages of the other two species detected (Fe_3O_4 and paramagnetic Fe^{2+}) are equal too. Therefore, it can be concluded that in both atmospheres, just about 10% of the total iron loading can be reduced beyond Fe_3O_4 or Fe^{2+}. On the other hand, the activation atmosphere has a decisive role to determine whether the more reduced iron species present in the fresh catalysts – zero reaction time – is α-Fe or χ-Fe_2C_5 carbide. Finally, an important diffusion process of the iron ions inside the SBA-15 lattice occurs during the activation steps in both atmospheres, since in the precursor, only 4% of the total iron loading had diffused inside the SBA-15 walls.

The Mössbauer spectra of the used catalysts under the FTS conditions for 24 h (pseudo-stationary state) (Fig. 6) do not show important differences either between them or with respect to the fresh solids when they were measured at 298 K. Both of them display an asymmetric doublet with a shoulder on the positive-velocity side and broad lines, which could be attributed to paramagnetic and/or superparamagnetic (sp) species. However, when the Mössbauer spectra at 30 K were obtained, some changes appeared. The spectra were fitted following the methodology previously described with the fresh catalysts. Again, the used H2:CO–Fe/SBA-15 spectrum at 30 K was fitted with five sextets for the five Fe_3O_4 crystallographic sites [43], four sextets assigned to the three sites of the χ-Fe_2C_5 carbide [44] and the two sites of the ε'-$Fe_{2.2}C$ carbide [47], and two doublets assigned to Fe^{2+} ions located in tetrahedral and octahedral sites within the walls of SiO_2 [45] (Table 6 and Fig. 6). It is important to remark that it was necessary to add another sextet, in comparison with the fresh catalyst, in order to obtain a satisfactory fitting. The new sextuplet was assigned to the II crystallographic site of the ε'-$Fe_{2.2}C$ carbide. The I site of this carbide shows an overlapped signal with the II site of the χ-Fe_2C_5 carbide. Taking into account these assignments, it can be concluded

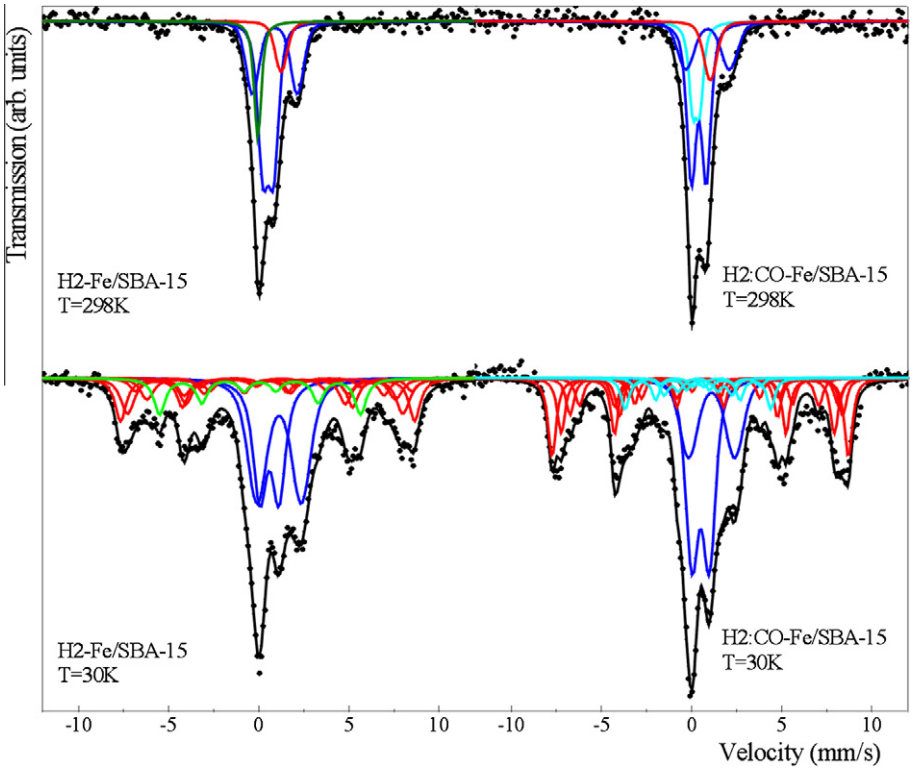

Fig. 5. Mössbauer spectra of H2-Fe/SBA-15 and H2:CO–Fe/SBA-15 at zero reaction time (fresh catalysts) in controlled atmosphere at 298 and 30 K.

Table 4
Mössbauer parameters in controlled atmosphere at 298 and 30 K of H2-Fe/SBA-15 and H2:CO–Fe/SBA-15 at zero reaction time (fresh catalysts).

Temperature (K)	Species	Parameters[a]	H2-Fe/SBA-15	H2:CO–Fe/SBA-15
298	χ carbide (sp)	Δ (mm/s)	–	0.4 ± 0.1
		δ (mm/s)	–	0.3 ± 0.1
	α-Fe (sp)	δ (mm/s)	0.06 ± 0.04	–
	Fe^{2+} in silica octahedral sites	Δ (mm/s)	2.5 ± 0.1	2.4 ± 0.2
		δ (mm/s)	0.89 ± 0.04	0.90 ± 0.09
	Fe^{2+} in silica tetrahedral sites	Δ (mm/s)	0.60 ± 0.09	0.8 ± 0.1
		δ (mm/s)	0.52 ± 0.07	0.41 ± 0.04
	Fe_3O_4 (sp)	δ (mm/s)	1.2 ± 0.2	1.0 ± 0.2
30	χ carbide-site I	H (T)	–	21.7[b]
	χ carbide-site II	H (T)	–	25.1 ± 0.5
	χ carbide-site III	H (T)	–	11.7[b]
	α-Fe	H (T)	34.6 ± 0.4	–
	Fe_3O_4-site I	H (T)	47.4 ± 0.9	47.0 ± 0.3
	Fe_3O_4-site II	H (T)	50.6 ± 0.5	51.0 ± 0.2
	Fe_3O_4-site III	H (T)	43 ± 1	44.5 ± 0.6
	Fe_3O_4-site IV	H (T)	48 ± 2	46.9 ± 0.5
	Fe_3O_4-site V	H (T)	34.4 ± 0.9	35.1 ± 0.5
	Fe^{2+} in silica octahedral sites	Δ (mm/s)	2.46 ± 0.09	2.6 ± 0.1
		δ (mm/s)	1.13 ± 0.05	1.1 ± 0.1
	Fe^{2+} in silica tetrahedral sites	Δ (mm/s)	1.06 ± 0.08	0.96 ± 0.05
		δ (mm/s)	0.59 ± 0.04	0.51 ± 0.03

H: hyperfine magnetic field in Tesla.
δ: isomer shift (all the isomer shifts are referred to α-Fe at 298 K).
2ε: quadrupole shift.
Δ: quadrupole splitting.
[a] Hyperfine parameters.
[b] Parameters held fixed in fitting.

that at 298 K, the iron species are present in a superparamagnetic regime and as paramagnetic species. Therefore, while the H2:CO–Fe/SBA-15 catalyst is "working", important crystal size changes do not occur and the more remarkable change is the ε'-$Fe_{2.2}C$ carbide appearance, while the percentage of magnetite remains nearly constant (Table 7). The used H2-Fe/SBA-15 spectrum at 30 K was fitted with two sextets for the Fe_3O_4, four sextets assigned to the three sites of the χ-Fe_2C_5 carbide and the two sites of the ε'-$Fe_{2.2}C$ carbide, and two doublets assigned to Fe^{2+} ions located in tetrahedral and octahedral sites within the walls of SiO_2 (Table 6 and Fig. 6). Note that only two sextuplets were used in order to fit the Fe_3O_4 signals: one of them represents an average weight

Table 5
Iron species percentages in the activated catalysts – zero reaction time – obtained from the Mössbauer spectra in controlled atmosphere evaluated at 30 K.

Species (%)	H2-Fe/SBA-15	H2:CO–Fe/SBA-15
α-Fe	11 ± 2	–
Fe^{2+}	47 ± 4	41 ± 3
Fe_3O_4	42 ± 13	47 ± 8
χ-Fe_2C_5	–	12 ± 6

of the Fe^{3+} populations and the other an average weight of the Fe^{2+} populations. This procedure was chosen taking into account that the Fe_3O_4 percentage decreased with respect to the fresh catalyst (42 ± 13 vs. 27 ± 2). Therefore, it is not advisable to use many interactions to distinguish the different crystallographic sites in a poorly defined signal. In the same way as in H2:CO–Fe/SBA-15, no sintering occurs while H2-Fe/SBA-15 is "working". However, one important structural change happens, and the α-Fe species disappears completely to produce a mixture of χ-Fe_2C_5 and ε'-$Fe_{2.2}C$ carbide. Therefore, both catalysts "working" under FTS conditions have the same iron species. Other authors have found that the "working" catalysts are a mixture of Fe carbides and oxides [4–6,48–50]. Unfortunately, the large errors of the areas – produced by the great overlapping of the signals – prevent a precise evaluation of the content of these species (Table 7). However, it is difficult to justify the great differences in the catalytic behavior between both solids at lower differences in the content of the same iron species.

Therefore, in order to explain these results, the TPH assays on both catalysts – after 6 days of continuous reaction – were performed (Fig. 7). This technique was selected since, as was clearly demonstrated by Xu and Bartholomew [20], it allows identifying carbon species of different structures and reactivities and different iron carbides. Two peaks assignable to ε'-$Fe_{2.2}C$ (884 K) and χ-Fe_5C_2 (955 K) carbides [20] can be clearly identified in H2-Fe/SBA-15 (Fig. 7), in agreement with the Mössbauer results. The same species were identified in H2:CO–Fe/SBA-15. However, both peaks showed a shift toward higher temperatures of about 80 K. This behavior would indicate that the iron carbides produced in this catalyst are more stable and therefore less reactive than those produced in H2-Fe/SBA-15.

For many years, the possibility that carbon atoms on the catalyst surface become incorporated into reaction products has been considered [51]. However, only recently, calculations using the density functional theory would indicate that the C necessary to produce CH_4 and hydrocarbons "gets away" from the carbide surfaces [52]. The presence of these empty sites enhances CO adsorption and largely lowers the CO dissociation energy barrier. Therefore, the vacancies are refilled with new CO molecules that are dissociated, and the active carbide surface is regenerated. Simultaneously, with this publication appeared a work of Niemantsverdriet's group [53] in which, using a similar model starting from the Fe_5C_2 (1 0 0) surface, they concluded that the mechanism starts with the exothermic hydrogenation of a surface carbidic carbon to CH_3. This liberates a site of 4-fold coordination between iron atoms, which becomes available for CO adsorption. This adsorbed CO is dissociated – assisted by hydrogen – in a carbidic C atom and an OH group. The latter process restores the carbide surface, while the OH group forms water and CH_3 forms methane. These authors envisage the overall reaction cycle as a Mars-van Krevelen mechanism for catalytic oxidation reactions.

Both articles would explain why if more reactive iron carbides are obtained (as occurs when pure H_2 is used in the activation process with the Fe/SBA-15 system), a more active catalyst is produced. In agreement with this description, in H2:CO–Fe/SBA-15, a third peak at higher temperature (1141 K) assigned to graphite carbon [20] was detected in the TPH diagram. The cycle previously described would be slower on the surface of the less reactive iron

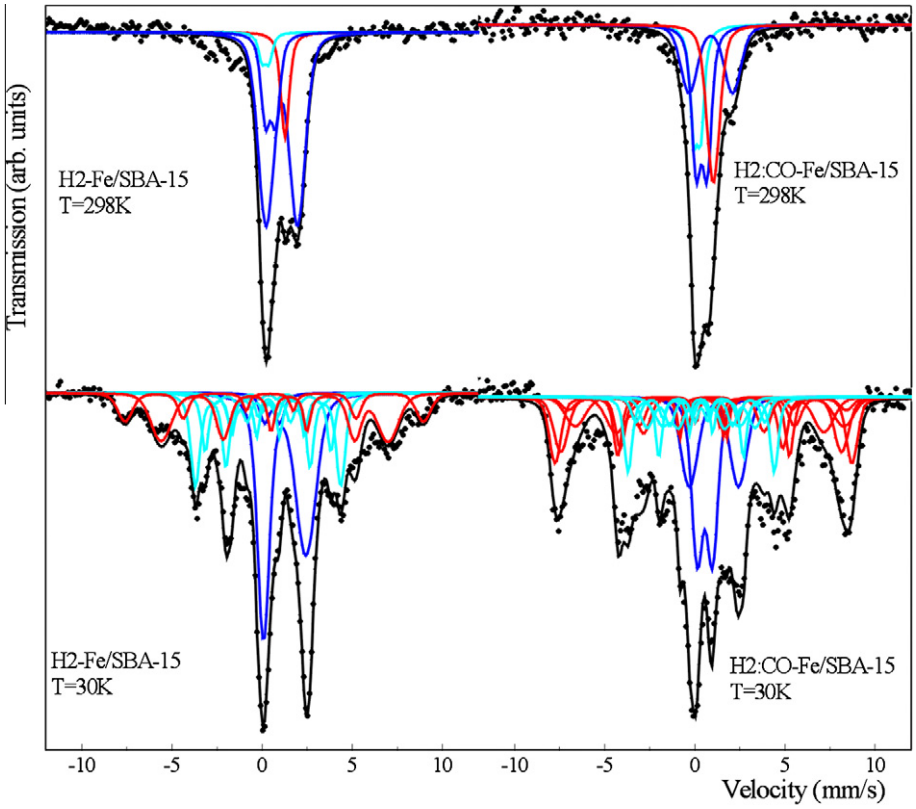

Fig. 6. Mössbauer spectra of H2-Fe/SBA-15 and H2:CO–Fe/SBA-15 in the pseudo-stationary state (≈24 h) (used catalysts) in controlled atmosphere at 298 and 30 K.

Table 6
Mössbauer parameters in controlled atmosphere at 298 and 30 K of H2-Fe/SBA-15 and H2:CO–Fe/SBA-15 in the pseudo-stationary state (≈24 h) (used catalysts).

Temperature (K)	Species	Parameters[a]	H2-Fe/SBA-15	H2:CO–Fe/SBA-15
298	($\chi + \varepsilon'$) carbide (sp)	Δ (mm/s)	0.4 ± 0.1	0.39[b]
		δ (mm/s)	0.2 ± 0.1	0.14 ± 0.06
	Fe^{2+} in silica octahedral sites	Δ (mm/s)	1.75 ± 0.06	2.4 ± 0.1
		δ (mm/s)	1.09 ± 0.03	0.89 ± 0.06
	Fe^{2+} in silica tetrahedral sites	Δ (mm/s)	0.57 ± 0.08	0.61 ± 0.07
		δ (mm/s)	0.47 ± 0.07	0.38 ± 0.04
	Fe_3O_4 (sp)	δ (mm/s)	1.27 ± 0.04	1.03 ± 0.07
30	χ carbide-site I	H (T)	21.6 ± 0.2	22 ± 1
	χ carbide-site II + ε' carbide-site I	H (T)	25.0 ± 0.1	25.2 ± 0.3
	χ carbide-site III	H (T)	12.8[b]	13.3[b]
	ε' carbide-site II	H (T)	18.6[b]	19 ± 1
	Fe_3O_4-site I	H (T)	–	48.3 ± 0.5
	Fe_3O_4-site II	H (T)	–	51.1 ± 0.3
	Fe_3O_4-site III	H (T)	–	47.8[b]
	Fe_3O_4-site IV	H (T)	–	46.2[b]
	Fe_3O_4-site V	H (T)	–	35.7 ± 0.6
	Fe_3O_4 weight average of sites I–III	H (T)	51.3 ± 0.4	–
	Fe_3O_4 weight average of sites IV and V	H (T)	39.0 ± 0.3	–
	Fe^{2+} in silica octahedral sites	Δ (mm/s)	2.35 ± 0.03	2.73 ± 0.08
		δ (mm/s)	1.26 ± 0.02	1.07 ± 0.05
	Fe^{2+} in silica tetrahedral sites	Δ (mm/s)	0.84[b]	0.84 ± 0.03
		δ (mm/s)	0.56[b]	0.56 ± 0.02

H: hyperfine magnetic field in Tesla.
δ: isomer shift (all the isomer shifts are referred to α-Fe at 298 K).
2ε: quadrupole shift.
Δ: quadrupole splitting.
[a] Hyperfine parameters.
[b] Parameters held fixed in fitting.

Table 7
Iron species percentages in the used catalysts 24 h – pseudo-stationary state – obtained from the Mössbauer spectra in controlled atmosphere evaluated at 30 K.

Species (%)	H2-Fe/SBA-15	H2:CO–Fe/SBA-15
Fe^{2+}	34 ± 2	26 ± 2
Fe_3O_4	27 ± 2	47 ± 10
χ-Fe_2C_5 + ε'-$Fe_{2.2}C$	39 ± 5	27 ± 8

carbides produced in H2:CO–Fe/SBA-15. Therefore, the *C* could remain more time on the surface, allowing its polymerization, and producing – after a long reaction time – graphitic carbon. The steps of the process are schematically described in Fig. 8.

Another question appears from the present results: why the same iron carbides produced by different processes show different reactivities. Taking into account that the Fe_5C_2 (1 0 0) surface has the highest carbon content and therefore will exhibit the lowest reactivity toward CO [53], we can speculate that different iron carbide plane populations will be obtained if different activation processes are used. Therefore, when the H_2:CO mixture is used as activation gas, the (1 0 0) surface carbide would be predominant in the Fe/SBA-15 system.

An alternative explanation can be envisaged considering the sequential phase modifications from α-Fe_2O_3 to "working" catalysts. Using the sequences reported by Iglesia's group [39,54] for promoted unsupported precipitated iron catalysts and by Xu and Bartholomew [20] for iron supported on amorphous silica, the following steps could be proposed. The very small α-Fe_2O_3 "nanocylinders" undergo a fast reduction to Fe_3O_4 with either H_2 or H_2:CO pretreatment. The next step would produce – with a lower reduction rate – a thin "shell" of α-Fe with a "core" of Fe_3O_4, when pure H_2 is used. Instead, H_2:CO produces – with a slow rate too – very small "seeds" of χ-Fe_5C_2 on the surface of Fe_3O_4 "nanocylinders". The later description is based on previous TEM studies in which it was demonstrated that the surface iron carbides FeC_x grow up as small "nodules" on the surface of the crystals independently

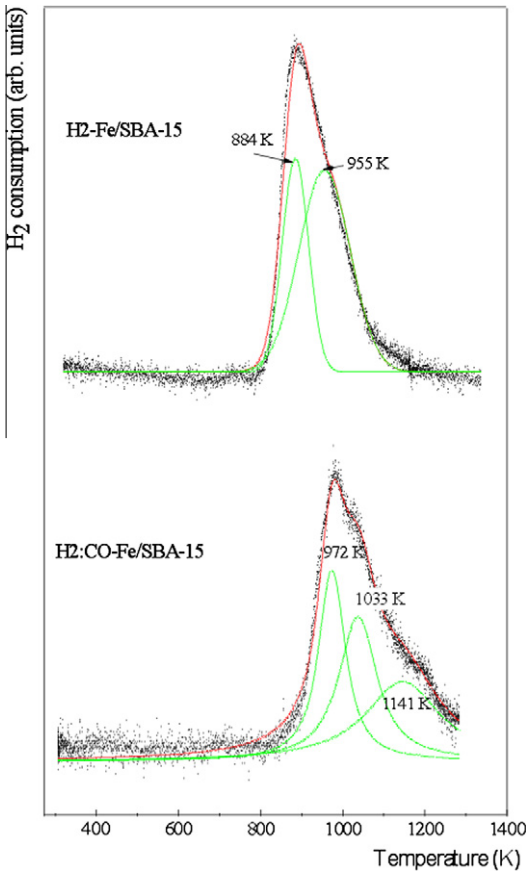

Fig. 7. TPH of H2-Fe/SBA-15 and H2:CO–Fe/SBA-15 after 6 days under continuous FTS conditions.

of the "core" nature [11,55]. While the H2:CO–Fe/SBA-15 catalyst is "working", slight changes occur; the percentage of iron carbides

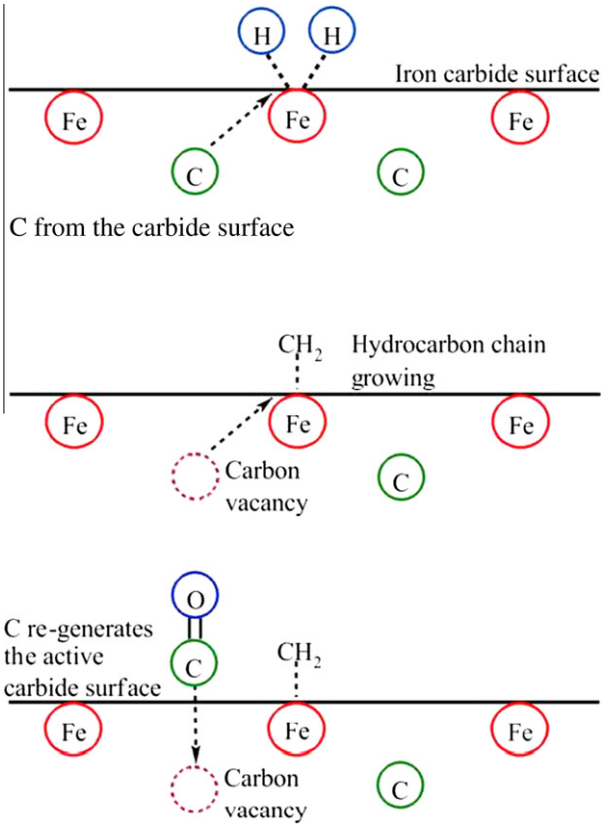

Fig. 8. Schematic representation of the overall reaction cycle.

increases and ε′-$Fe_{2.2}C$ carbide appears. However, when H2-Fe/SBA-15 is contacted with syngas, a large number of FeC_x "nodules" would appear quickly on the α-Fe "shell". The different carburization velocities between Fe_3O_4 (H2:CO–Fe/SBA-15) and [α-Fe "shell" + Fe_3O_4 "core"] (H2-Fe/SBA-15) nanocrystals could be explained since the rate of carburization of metal oxides is controlled by oxygen diffusion from the oxide "core" to its surface [56]. This step does not occur when Fe_3O_4 nanocrystals are covered by a "shell" of α-Fe. As a consequence, a larger number of these "nodules", of a smaller size, could be obtained on the surface of the [α-Fe "shell" + magnetite "core"] crystals than on the surface of magnetite. Therefore, a larger number of sites for CO adsorption and dissociation and shorter diffusion paths would be obtained when pure H_2 is used in the activation treatment and the catalyst will be more active. This conclusion takes into account the fact that the surface areas of small "nodules" with FeC_x composition in surface layers control the FTS rates independently of the chemical nature of the residual oxide or carbide "cores" [39]. In the same way, these carbide "nodules" would be more unstable in contact with pure H_2 during TPH experiments, and decomposition peaks at lower temperatures will be obtained. In Fig. 9, a schematic picture of these steps is shown.

The existence of a very thin "shell" of α-Fe on the surface of the nanometric Fe_3O_4 "core" and very small "nodules" of carbides is consistent with the superparamagnetic behavior showed by these species in the Mössbauer spectra at 298 K in fresh and used catalysts.

Both points of view could be reconciled if we imagine that H_2 activation would produce a larger number of smaller iron carbide "nodules" with a lower number of (1 0 0) surfaces exposed to reactive gases.

4. Conclusions

An iron catalyst supported on a mesoporous solid SBA-15 has been prepared. The total iron loading was located inside the channels of the support. In consequence, very small iron oxide particles with a narrow size distribution were obtained. These characteristics of the iron species sizes were preserved after the activation process and while the catalysts were "working".

The precursor was activated using two different methodologies: with pure H_2 and with a mixture of H_2:CO (2:1). The different activation treatments led to different Fe species in the fresh catalysts: α-Fe, Fe_3O_4, and Fe^{2+} diffused into the SBA-15 walls in H2-Fe/SBA-15 and χ-Fe_5C_2 carbide, Fe_3O_4, and Fe^{2+} in H2:CO–Fe/SBA-15. These initial differences in the "bulk" structure of the solids disappear when both catalysts are "working" under the FTS conditions. However, a higher production of total hydrocarbons, higher CO conversion, and more CH_4 and light gases were obtained over 6 days of

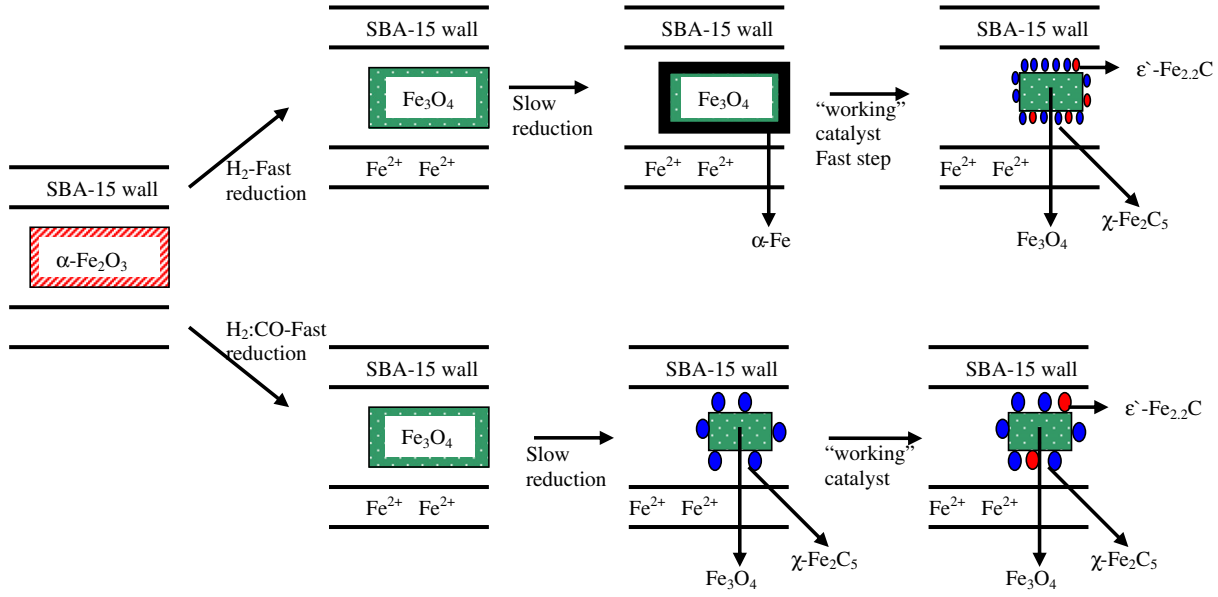

Fig. 9. Schematic representation of the sequential phase modifications from precursor to "working" catalysts depending on the activation atmospheres.

continuous reaction when the activation in pure H_2 was performed. Besides, a higher selectivity toward light olefins was obtained with the same solid during the first 24 h of reaction stream, but this selectivity decreases with the reaction time. At long reaction time (≈144 h), definitive conclusions about this aspect of the selectivity cannot be obtained due to the differences in CO conversion.

These results are explained taking into account that the iron carbides produced from α-Fe are more reactive than that obtained from Fe_2O_3 in a direct way (activations in pure H_2 and H_2:CO mixture respectively). We speculate that when the iron carbides are obtained from iron oxide in a direct way, planes with the highest carbon content (and therefore with the lowest reactivity toward CO) are predominant. A different velocity of iron carbide "nodule" production on the surface of the nanocrystals – depending on whether this appearance occurs on the Fe_3O_4 surface or the α-Fe "shell" – could produce a larger number of these "nodules" with smaller sizes in the latter case. Therefore, a larger number of sites for CO adsorption and dissociation and shorter diffusion paths would be obtained, and the catalyst will be more active. A combination of both effects would also be possible.

An active surface instead of an active site would exist in this model. This active surface is "alive", changing and regenerating all the time while the catalysts are "working" under the FTS conditions.

Taking into account that the literature data related to the activation process of the iron catalysts to be used in the FTS are contradictory and strongly depend on the catalyst characteristics (supported or not, with promoters or not, etc.), at the moment it does not seem appropriate to perform a generalization on this topic. Instead, a study for each Fe system in particular appears more advisable.

Acknowledgments

The authors acknowledge the financial support of ANPCyT (PICT No. 22-38337 and 00549), which allowed the development of this work.

References

[1] A. Steynberg, M. Dry (Eds.), Fischer–Tropsch Technology, Stud. Surf. Sci. Catal., Elsevier, Amsterdam, 2004.
[2] B.H. Davis, M.L. Occelli (Eds.), Fischer–Tropsch Synthesis, Catalysts and Catalysis, Stud. Surf. Sci. Catal., Elsevier, Amsterdam, 2007.
[3] M. Luo, H. Hamdeh, B.H. Davis, Catal. Today 140 (2009) 127.
[4] R.B. Anderson, The Fischer–Tropsch Synthesis, Academic Press, Orlando, FL, 1984.
[5] J.A. Amelse, J.B. Butt, L.H. Schwartz, J. Phys. Chem. 82 (1978) 558.
[6] G.B. Raupp, W.N. Delgass, J. Catal. 58 (1979) 361.
[7] J.W. Niemantsverdriet, A.M. van der Kraan, J. Catal. 72 (1981) 385.
[8] J.P. Reymond, P. Meriadeau, S.J. Teichner, J. Catal. 75 (1982) 39.
[9] F. Blanchard, J.P. Reymond, B. Pommier, S.J. Teichner, J. Mol. Catal. 17 (1982) 171.
[10] R. Dictor, A.T. Bell, J. Catal. 97 (1986) 121.
[11] M.D. Shroff, D.S. Kalakkad, K.E. Coulter, S.D. Köhler, M.S. Harrington, N.B. Jackson, A.G. Sault, A.K. Datye, J. Catal. 156 (1995) 185.
[12] S. Soled, E. Iglesia, R.A. Fiato, Catal. Lett. 7 (1990) 271.
[13] C.S. Kuivila, P.C. Stair, J.B. Butt, J. Catal. 118 (1989) 299.
[14] J.B. Butt, Catal. Lett. 7 (1990) 61.
[15] H.W. Pennline, M.F. Zarochak, J.M. Stencel, J.R. Diehl, Ind. Eng. Chem. Res. 26 (1987) 595.
[16] D.B. Bukur, L. Nowicki, R.K. Manne, X. Lang, J. Catal. 155 (1995) 366.
[17] D.B. Bukur, L. Nowicki, X. Lang, Catal. Today 24 (1995) 111.
[18] R.J. O'Brien, L. Xu, R.L. Spicer, B.H. Davis, Energy Fuels 10 (1996) 921.
[19] R.J. O'Brien, L. Xu, R.L. Spicer, S. Bao, D.R. Milburn, B.H. Davis, Catal. Today 36 (1997) 325.
[20] J. Xu, C.H. Bartholomew, J. Phys. Chem. B 109 (2005) 2392.
[21] M. Boudart, A. Delbouille, J.A. Dumesic, S. Khammouma, H. Topsøe, J. Catal. 37 (1975) 486.
[22] M.A. McDonald, D.A. Storm, M. Boudart, J. Catal. 102 (1986) 386.
[23] E.I. Mabaso, E. van Steen, M. Claeys, DGMK, Tagungsbericht 4 (2006) 93.
[24] L.A. Cano, M.V. Cagnoli, N.A. Fellenz, J.F. Bengoa, N.G. Gallegos, A.M. Alvarez, S.G. Marchetti, Appl. Catal. A 379 (2010) 105.
[25] P.B. Radstake, J.P. den Breejen, G.L. Bezemer, J.H. Bitter, K.P. de Jong, V. Frøseth, A. Holmen, Stud. Surf. Sci. Catal. 167 (2007) 85.
[26] G.L. Bezemer, J.H. Bitter, H.P.C.E. Kuipers, H. Oosterbeek, J.E. Holewijn, X. Xu, F. Kapteijn, A.J. van Dillen, K.P. de Jong, J. Am. Chem. Soc. 128 (12) (2006) 3956.
[27] D. Zhao, J. Feng, Q. Huo, N. Melosh, G.H. Fredrickson, B.F. Chmelka, G.D. Stucky, Science 279 (1998) 23.
[28] D. Zhao, Q. Huo, J. Feng, B.F. Chmelka, G.D. Stucky, J. Am. Chem. Soc. 120 (1998) 6024.
[29] K. Lagarec, D.G. Rancourt, Mossbauer Spectral analysis Software, Dep. of Phys. University of Otawa, Version 1.0., 1998.
[30] S.G. Marchetti, J.F. Bengoa, M.V. Cagnoli, A.M. Alvarez, N.G. Gallegos, A.A. Yeramián, R.C. Mercader, Meas. Sci. Technol. 7 (1996) 758.
[31] J.S. Beck, J.C. Vartuli, W.J. Roth, M.E. Leonowicz, C.T. Kresge, K.D. Schmidt, C.T.W. Chu, D.H. Olson, E.W. Sheppard, S.B. McCullen, J.B. Higgins, J.L. Schlenker, J. Am. Chem. Soc. 114 (1992) 10834.
[32] J.R.A. Sietsma, J.P. den Breejen, P.E. de Jongh, A.J. van Dillen, J.H. Bitter, K.P. de Jong, Stud. Surf. Sci. Catal. 167 (2007) 55.
[33] J.P. den Breejen, J.R.A. Sietsma, H. Friedrich, J.H. Bitter, K.P. de Jong, J. Catal. 270 (2010) 146.
[34] E. Murad, J.H. Johnston, in: G.J. Long (Ed.), Mössbauer Spectroscopy Applied to Inorganic Chemistry, vol. 2, Plenum Publishing Corporation, 1987.
[35] R.E. Vandenberghe, E. De Grave, C. Landuydt, L.H. Bowen, Hyperfine Interact 53 (1990) 175.
[36] M. Blume, J.A. Tjon, Phys. Rev. 165 (1968) 446.
[37] W.F. Brown Jr., Phys. Rev. 130 (1963) 1677.
[38] F. Bødker, S. Mørup, Europhys. Lett. 52 (2000) 217.
[39] S. Li, W. Ding, G.D. Meitzner, E. Iglesia, J. Phys. Chem. B 106 (2002) 85.
[40] J.F. Bengoa, M.V. Cagnoli, N.G. Gallegos, A.M. Alvarez, L.V. Mogni, M.S. Moreno, S.G. Marchetti, Micropor. Mesopor. Mater. 84 (2005) 153.
[41] M.S. Moreno, M. Weyland, P.A. Midgley, J.F. Bengoa, M.V. Cagnoli, N.G. Gallegos, A.M. Alvarez, S.G. Marchetti, Micron 37 (2006) 52.
[42] M. Röper, in: W. Keim (Ed.), Catalysis in C1 Chemistry, D. Reidel Publishing Company, Dordrecht, Boston, Lancaster, 1983, p. 41.
[43] F.J. Berry, S. Skinner, M.F. Thomas, J. Phys.: Condens. Matter. 10 (1998) 215.
[44] S.-Ch. Lin, J. Phillips, J. Appl. Phys. 58 (5) (1985) 1943.
[45] B.S. Clausen, H. Topsøe, S. Mørup, Appl. Catal. 48 (1989) 327.
[46] S. Mørup, H. Topsøe, J. Lipka, J. Phys. Colloq. 37 (1976) C6–287.
[47] M. Pijolat, V. Perrichón, P. Bussiére, J. Catal. 107 (1987) 82.
[48] R.B. Anderson, in: P.H. Emmett (Ed.), Catalysis, forth ed., Van Nostrand-Reinhold, New York, 1956, p. 29.
[49] M.E. Dry, in: J.R. Anderson, M. Boudart (Eds.), Catalysis: Science and Technology, vol. 1, Springer, New York, 1981, p. 159.
[50] C.N. Satterfield, R.T. Hanlon, S.E. Tung, Z. Zou, G.C. Papaefthymiou, Ind. Eng. Chem. Prod. Dev. 25 (1986) 407.
[51] H. Matsumoto, C.O. Bennett, J. Catal. 53 (1978) 331.
[52] Ch.-F. Huo, Y.-W. Li, J. Wang, H. Jiao, J. Am. Chem. Soc. 131 (2009) 14713.
[53] J.M. Gracia, F.F. Prinsloo, J.W. Niemantsverdriet, Catal. Lett. 133 (2009) 257.
[54] S. Li, G.D. Meitzner, E. Iglesia, J. Phys. Chem. B 105 (2001) 5743.
[55] N.B. Jackson, A.K. Datye, L. Mansker, R.J. O'Brien, B.H. Davis, Stud. Surf. Sci. Catal. 111 (1997) 501.
[56] S.T. Oyama, J.C. Schlatter, J.E. Metcalfe, J.M. Lambert Jr., Ind. Eng. Chem. Res. 27 (1988) 1639.